33RD INTERNATIONAL COSMIC RAY CONFERENCE, RIO DE JANEIRO 2013
THE ASTROPARTICLE PHYSICS CONFERENCE

ICRC 2013

Hydrogen and helium isotopes flux in cosmic rays with the PAMELA experiment

V. FORMATO[8,15], O. ADRIANI[1,2], G.C. BARBARINO[3,4], G.A. BAZILEVSKAYA[5], R. BELLOTTI[6,7], M. BOEZIO[8], E.A. BOGOMOLOV[9], M. BONGI[1,2], V. BONVICINI[8], S. BOTTAI[2], A. BRUNO[7], F. CAFAGNA[7], D. CAMPANA[4], R. CARBONE[8], P. CARLSON[10], M. CASOLINO[11,12], G. CASTELLINI[13], C. DE DONATO[10,11], M.P. DE PASCALE[11,14,*], C. DE SANTIS[11,14], N. DE SIMONE[11], V. DI FELICE[11], A.M. GALPER[16], A.V. KARELIN[16], S.V. KOLDASHOV[16], S. KOLDOBSKIY[16], Y. KRUTKOV[9], A.N. KVASHNIN[5], A. LEONOV[16], V. MALAKHOV[16], L. MARCELLI[14], M. MARTUCCI[14,17] A.G. MAYOROV[16], W. MENN[18], M. MERGÈ[11,14] V.V. MIKHAILOV[16], E. MOCCHIUTTI[8], A. MONACO[7], N. MORI[2], R. MUNINI[8,15], G. OSTERIA[4], F. PALMA[11,14], P. PAPINI[2], M. PEARCE[10], P. PICOZZA[11,14], C. PIZZOLOTTO[19,20,†], M. RICCI[17], S.B. RICCIARINI[2], R. SARKAR[8], M. SIMON[18], V. SCOTTI[3,4], R. SPARVOLI[11,14], P. SPILLANTINI[1,2], Y.I. STOZHKOV[5], A. VACCHI[8], E. VANNUCCINI[2], G. VASILYEV[9], S.A. VORONOV[16], Y.T. YURKIN[16], G. ZAMPA[8], N. ZAMPA[8], V.G. ZVEREV[16]

[1] *University of Florence, Department of Physics, I-50019 Sesto Fiorentino, Florence, Italy*
[2] *INFN, Sezione di Florence, I-50019 Sesto Fiorentino, Florence, Italy*
[3] *University of Naples "Federico II", Department of Physics, I-80126 Naples, Italy*
[4] *INFN, Sezione di Naples, I-80126 Naples, Italy*
[5] *Lebedev Physical Institute, RU-119991, Moscow, Russia*
[6] *University of Bari, Department of Physics, I-70126 Bari, Italy*
[7] *INFN, Sezione di Bari, I-70126 Bari, Italy*
[8] *INFN, Sezione di Trieste, I-34149 Trieste, Italy*
[9] *Ioffe Physical Technical Institute, RU-194021 St. Petersburg, Russia*
[10] *KTH, Department of Physics, and the Oskar Klein Centre for Cosmoparticle Physics, AlbaNova University Centre, SE-10691 Stockholm, Sweden*
[11] *INFN, Sezione di Rome "Tor Vergata", I-00133 Rome, Italy*
[12] *RIKEN, Advanced Science Institute, Wako-shi, Saitama, Japan*
[13] *IFAC, I-50019 Sesto Fiorentino, Florence, Italy*
[14] *University of Rome "Tor Vergata", Department of Physics, I-00133 Rome, Italy*
[15] *University of Trieste, Department of Physics, I-34147 Trieste, Italy*
[16] *NRNU MEPhI, RU-115409 Moscow, Russia*
[17] *INFN, Laboratori Nazionali di Frascati, Via Enrico Fermi 40, I-00044 Frascati, Italy*
[18] *Universitat Siegen, Department of Physics, D-57068 Siegen, Germany*
[19] *INFN, Sezione di Perugia, I-06123 Perugia, Italy*
[20] *Agenzia Spaziale Italiana (ASI) Science Data Center, I-00044 Frascati, Italy*
(*) Deceased
(†) Previously at INFN, Sezione di Trieste, I-34149 Trieste, Italy

valerio.formato@ts.infn.it

Abstract: PAMELA is a satellite borne experiment designed to study with great accuracy cosmic rays of galactic, solar, and trapped nature, with particular focus on the antimatter component. The detector consists of a permanent magnet spectrometer core to provide rigidity and charge sign information, a Time-of-Flight system for velocity and charge information, a Silicon-Tungsten calorimeter and a Neutron detector for lepton/hadron identification. The beta and rigidity information allow to identify isotopes for $Z = 1$ and $Z = 2$ particles in the energy range 100 MeV/n to 1 GeV/n. In this work we will present the final PAMELA results on the H and He isotope fluxes measured during the 23rd solar minimum from 2006 to 2007. Such fluxes carry relevant information helpful in constraining parameters in galactic cosmic rays propagation models complementary to those obtained from other secondary to primary measurements such as the boron-to-carbon ratio.

Keywords: icrc2013, cosmic-rays, galactic propagation.

1 Introduction

Hydrogen and helium isotopes in cosmic rays are generally believed to be of secondary origin, resulting from the nuclear interactions of primary cosmic-ray protons and ^{4}He with the interstellar medium. A precise measurement of the isotopic composition of hydrogen and helium could provide important information about the propagation of cosmic rays in the interstellar space, since they offer better statistics than other secondaries. This can be crucial for the analysis of positron and antiproton spectra, which is the primary goal of several current cosmic-ray experiments [12, 13].

The PAMELA experiment has been measuring since July 2006 hydrogen and helium isotopes over a wide range of time with reduced instrumental uncertainty and with no environmental systematics, such as the residual atmosphere present in balloon experiments.

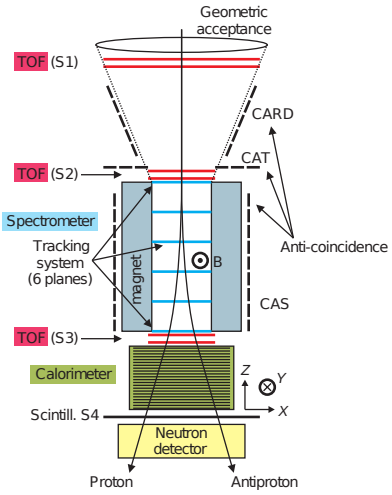

Fig. 1: A schematic overview of the PAMELA satellite experiment. The experiment stands ∼1.3 m high and, from top to bottom, consists of a time-of-flight (ToF) system (S1, S2, S3 scintillator planes), an anticoincidence shield system, a permanent magnet spectrometer (the magnetic field runs in the y-direction), a silicon-tungsten electromagnetic calorimeter, a shower tail scintillator (S4) and a neutron detector.

In this paper the isotopic composition is presented between 100 and 600 MeV/n for hydrogen isotopes and between 100 and 900 MeV/n for helium isotopes over the 23rd solar minimum from July 2006 to December 2007.

2 The PAMELA apparatus

PAMELA [9] is constituted by a number of redundant detectors (see Fig. 1) capable of identifying particles providing charge, mass, rigidity ($\rho = p/Ze$) and velocity ($\beta = v/c$) over a very wide energy range. Its main scientific objective is the study of the antimatter component in CR, see [**?**]. The core of the instrument is a permanent magnet with six planes of silicon microstrip detectors for tracking particles. A three-scintillators system provides trigger, charge and time of flight information. A silicon-tungsten calorimeter is used for hadron/lepton separation with a shower tail catcher and a neutron detector at the bottom of the apparatus to help increase this separation. An anticounter system is used to reject spurious events in the off-line phase. The readout electronics, the interfaces with the CPU and all primary and secondary power supplies are housed around the detectors. All systems (power supply, readout boards etc.) are redundant with the exception of the CPU which is more tolerant to failures. The apparatus is enclosed in a pressurized container located on one side of the Resurs-DK1 satellite. Total weight of PAMELA is 470 kg; power consumption is 355 W. A more detailed description of the instruments and the data handling can be found in [9].

3 Data Analysis

We adopted the same event selections as in previous works on the high energy proton and helium fluxes [1] and on the time dependence of the low energy proton flux [2].

These selections were developed in order to ensure a reliable event reconstruction and to select positively charged particles with a precise measurement of the absolute value of the particle rigidity and velocity.

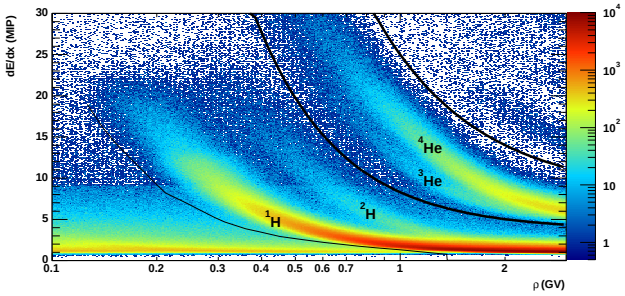

Fig. 2: Ionization energy loss in the magnetic spectrometer (mean of all planes hit). The black lines represent the selection for H and He nuclei.

Events with more than one track, likely to be products of hadronic interactions occurring in the top part of the apparatus, were rejected.

Furthermore the selected track must be at least 1.5 mm away from the magnet walls and the reconstructed curvature has to be consistent with positively-charged particles. Selected tracks must have at least four hits in the bending view of the spectrometer and three hits in the non-bending view.

In the two top planes of the ToF system there must be no more than one hit paddle and it must match with the extrapolated trajectory from the spectrometer. A positive ToF is requested to ensure that the particle enters PAMELA from above.

For hydrogen candidate events there must be no activity in the CARD and CAT scintillators of the anticoincidence system.

To select the primary (galactic) cosmic ray component particles were binned by requiring that $\rho_m > k \cdot G$, where G is the local geomagnetic cutoff evaluated in the Störmer approximation [11] using the IGRF magnetic field model [8], ρ_m is the lowest edge of the rigidity interval and $k = 1.3$ is a safety factor required to remove any directionality effects due to the Earth's penumbral regions.

3.1 Charge selection and Isotope reconstruction

The arithmetic mean of all the charge deposition in the spectrometer was used to select $Z = 1$ and $Z = 2$ particles applying a rigidity-dependent dE/dx selection, shown in Figure 2, which allows to have clean samples of H and He nuclei. In each sample different isotopic species can be distinguished due to the different velocity at a given rigidity

$$\beta = \left(1 + \frac{m^2}{Z^2\rho^2}\right)^{-1/2} \quad (1)$$

The event selection was performed in intervals of kinetic energy per nucleon. This implies that for each isotope different rigidity intervals have to be defined, as shown in Figure 3 where the $1/\beta$ distribution is shown for the energy interval 0.329-0.361 GeV/n in the ^{1}H and ^{2}H case. Particle counts were extracted from a Gaussian fit to the $1/\beta$ distribution in each rigidity range as shown by the solid lines in Figure 4. The reconstruction of helium isotopes was performed in a similar way, as shown in Figure 4 for

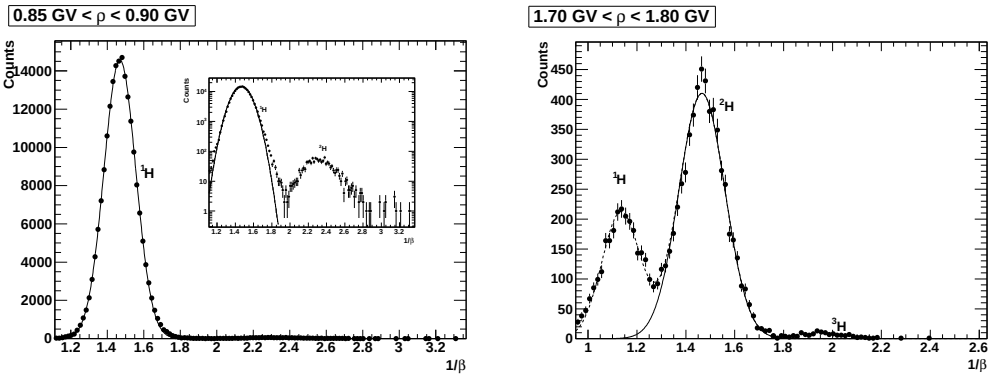

Fig. 3: Examples of $1/\beta$ distributions for the energy interval 0.329-0.361 GeV/n in the ^{1}H case (*left*) and in the ^{2}H case (*right*). The solid line shows the estimated ^{1}H and ^{2}H signal while the dashed line shows the combined fit used in the ^{2}H case to improve the fit result.

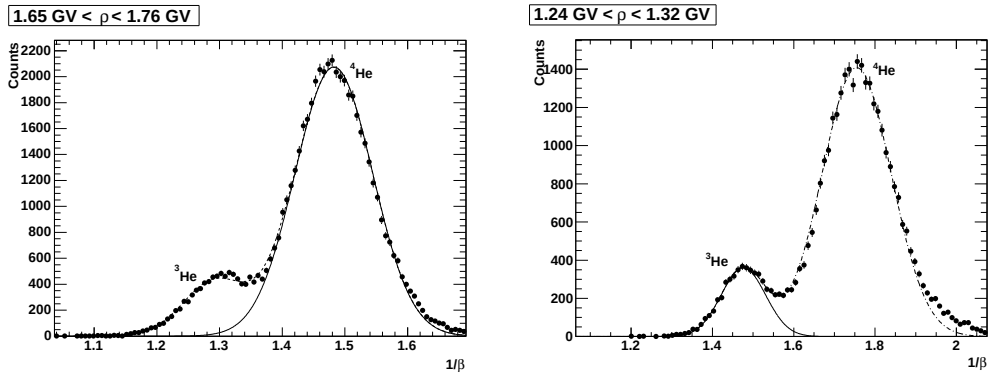

Fig. 4: Examples of $1/\beta$ distributions for the energy interval 0.312-0.350 GeV/n in the ^{4}He case (*left*) and in the ^{3}He case (*right*). The solid line shows the estimated ^{3}He and ^{4}He signal while the dashed line shows the combined fit used in the ^{3}He case to improve the fit result.

the energy interval 0.312-0.350 GeV/n. To help suppress the large proton (^{4}He) background in the ^{2}H (^{3}He) reconstruction two additional selections have been used, based on the lowest energy release among those provided by the tracking system and by the ToF system (only for ^{2}H reconstruction).

The reliability of the $1/\beta$ fits had been tested against a control sample built selecting ^{1}H and ^{2}H events not interacting in the electromagnetic calorimeter using a truncated mean of the calorimeter energy releases to separate the two species. The number of ^{1}H and ^{2}H reconstructed by the $1/\beta$ fit has been found in agreement with the number of events in the calorimeter sample.

3.2 Isotope Fluxes

To derive each isotope flux the number of selected events had to be corrected for the selections efficiencies, particle losses, contamination and energy losses. These corrections were obtained using a Monte Carlo simulation of the PAMELA apparatus based on the GEANT4 code [3] and from the flight data.

To correct the spectra distortion due to the resolution of the magnetic spectrometer and particle slowdown a Bayesian unfolding procedure, described in [7], was used to derive the number of events at the top of the payload (see [1]).

Fluxes were then derived according to the following definition

$$\Phi_{\mathrm{ToP}}(E) = \frac{N_{\mathrm{ToP}}(E)}{TG(E)\Delta E} \tag{2}$$

where $N_{\mathrm{ToP}}(E)$ is the unfolded particle count for energy E, also corrected for all the selection efficiencies, ΔE is the energy bin width, and $G(E)$ is the effective geometrical factor (accounting also for particle loss due to inelastic scattering), and T the live time.

4 Results

Figure 5 show hydrogen and helium isotope fluxes (top) and the ratios of the fluxes (bottom) while Figure 6 shows the ^{2}H/^{4}He ratio as a function of kinetic energy per nucleon, compared to previous measurements [4, 13, 10, 15, 14, 5].

The PAMELA results are the most precise to date. Considering the relatively large spread in the existing data, PAMELA results agree with previous measurements, in particular with BESS results for ^{2}H and IMAX results for ^{3}He. Previous measurements are affected by large uncertainties and, for ^{3}He where more measurements are available, there is a large spread between data. All the measurements displayed in Figures 5 and 6, except AMS-01, are from balloon-borne experiments and are affected by a non-negligible background of atmospheric secondary particles.

A high precision measurement of the H and He isotope quartet abundances represents a significant step forward in

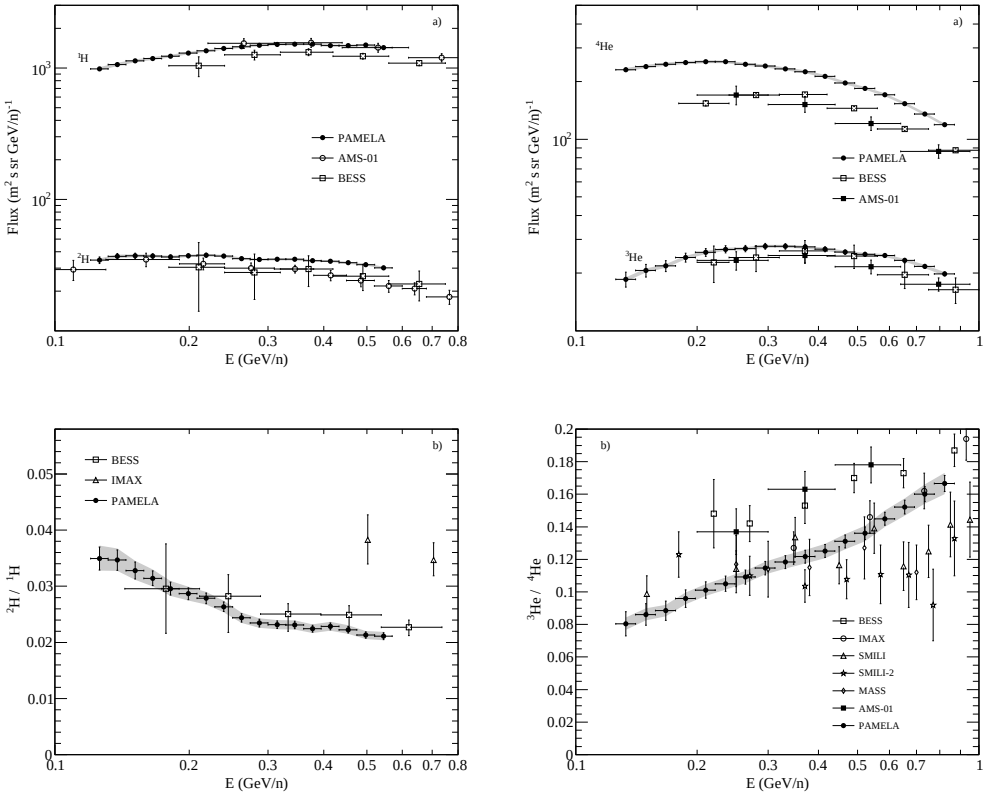

Fig. 5: *Left:* ^{1}H and ^{2}H absolute fluxes (a) and their ratio (b) compared to previous experiments: AMS-01 [4], BESS [13], IMAX [10]. *Right:* ^{4}He and ^{3}He absolute fluxes (a) and their ratio (b) compared to previous experiments: AMS [4], BESS [13], IMAX [10], SMILI-2[15], MASS [14], SMILI-1 [5]. Error bars show statistical uncertainty while shaded areas show systematic uncertainty.

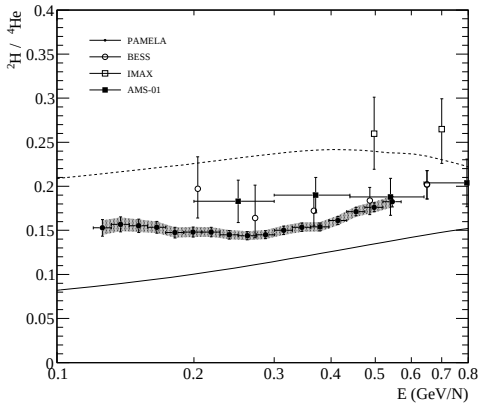

Fig. 6: ^{2}H/^{4}He ratio compared to previous experiments: AMS-01 [4], BESS [13], IMAX [10].

modelling the origin and propagation of GCRs. The constraints on diffusion-model parameters set by the quartet (^{1}H, ^{2}H, ^{3}He, and ^{4}He) were recently revisited [6]. It was found that the constraints on the parameters were competitive with those obtained from the B/C flux ratio analysis and available data supported the universality of GCR propagation in the Galaxy.

References

[1] Adriani, O., *et al.* 2011. *Science*, **332**, 69 - Supplementary Online Material.
[2] Adriani, O., *et al.* 2013, ApJ, 765, 91
[3] Agostinelli, S. et al., 2003, Nucl. Instrum. Meth. A, 506, 250
[4] Aguilar, M., *et al.* 2011. *ApJ*, **736**, 105.
[5] Beatty, J. J., *et al.* 1993. *ApJ*, **413**, 268.
[6] Coste, B., Derome, L., Maurin, D., & Putze, A. 2012. *Astronomy and Astrophysics*, **539**, A88.
[7] D'Agostini, G. 1995. *Nucl. Instrum. Meth.*, **A362**, 487.
[8] MacMillan, S., & Maus, S. 2005. *Earth, Planets, and Space*, **57**, 1135.
[9] Picozza, P., *et al.* 2007. *Astroparticle Physics*, **27**, 296.
[10] Reimer, O., *et al.* 1998. *ApJ*, **496**, 490.
[11] Shea, M. A., *et al.* 1987. *Physics of the Earth and Planetary Interiors*, **48**, 200–205.
[12] Stephens, S. A. 1989. *Advances in Space Research*, **9**, 145.
[13] Wang, J. Z., Seo, E. S., *et al.* . 2002. *ApJ*, **564**, 244.
[14] Webber, W. R., *et al.* 1991. *ApJ*, **380**, 230.
[15] Wefel, J. P., *et al.* 1995. International Cosmic Ray Conference, 2, 630.